Hue-assisted automatic registration of color point clouds

Hao Men and Kishore Pochiraju[*]

Department of Mechanical Engineering, Stevens Institute of Technology, Hoboken, NJ, 07030, USA

Abstract

This paper describes a variant of the extended Gaussian image based registration algorithm for point clouds with surface color information. The method correlates the distributions of surface normals for rotational alignment and grid occupancy for translational alignment with hue filters applied during the construction of surface normal histograms and occupancy grids. In this method, the size of the point cloud is reduced with a hue-based down sampling that is independent of the point sample density or local geometry. Experimental results show that use of the hue filters increases the registration speed and improves the registration accuracy. Coarse rigid transformations determined in this step enable fine alignment with dense, unfiltered point clouds or using Iterative Common Point (ICP) alignment techniques.

Keywords: Computational geometry; Mesh processing; Reverse engineering; Building information modeling (BIM); Computer graphics

---

1. Introduction

A number of 3D point cloud data registration techniques currently exist for generating accurate global maps by merging multiple point cloud maps from different vantage positions into a single global coordinate system [1]. In most cases 3D range points acquired from laser scanning devices contain detailed spatial information of the scanned environment saved with respect to the local coordinate reference frame defined by the scanned location and orientation. Creating an accurate global map from the individual point clouds scanned with local reference frames is an essential task for a number of different applications including construction / architectural surveying, area mapping, and autonomous robotic exploration.

If the scanner is precisely localized (location and pose are known), the registration is trivial. However, localizing a moving robot may be challenging or imprecise at best without the aid of locating beacons (e.g., GPS) and the localization errors translate to mapping errors. Registration algorithms analyze the scan data gathered from two locations for overlapping goemetry and use the geometric features to register a new unregistered point cloud (termed as the data cloud) into the reference frame of registered point clouds (model cloud). A well-known algorithm for 3D point cloud data registration is the Iterative Closest Point (ICP) [2] algorithm,

which has been applied to stitch two neighbor 3D point cloud maps into one map based on their overlap coverage area. Several variants of ICP are reported in the literature to increase the speed and precision [3]. Corresponding points ampling, matching, weighting and rejecting are some methods used to accelerate the ICP algorithm. In the ICP algorithm, associating corresponding points in two point cloud data sets is the most critical step.

Nearest neighbor search in 2D or 3D space is commonly used for associating the corresponding points. Parallel ICP algorithms have been developed [4] to accelerate computation speed. Point to plane registration method accelerates the ICP iteration and convergence [5]. A good initial (or rough) alignment with small translation and rotation errors is required for ICP [2]. Therefore, manual alignment often precedes the use of ICP.

Other techniques for registration include the point signature method [6] that used signature points to describe curvatures of point cloud data and matches corresponding signature points during the registration process. Spin image based methods compute 2D spin image to represent surface characterization and solve the registration problem by finding the best correspondence between two different scan spin images [7]. Methods such as the principle component analysis [8] and algebraic surface model [9] are based on matching the point cloud surface geometrical features.

Of these methods, the Extended Gaussian Image (EGI) based techniques [10] are capable of automatically performing rough alignment. EGI techniques determine the optimal rigid transformations that correlate the surface normal vector
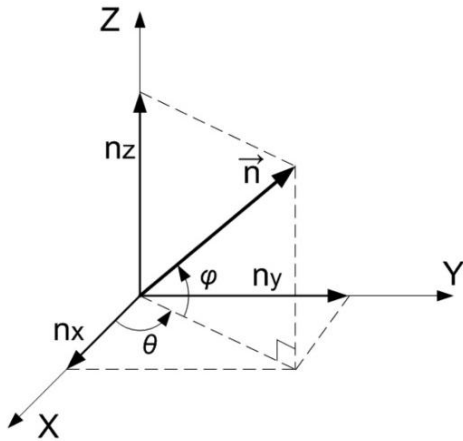

Figure 1. Surface normal orientation angle and vector.

distributions in the data and model point clouds. The rotation required to register two point clouds is solved using a cross-correlation function of the two EGI images. Computing the cross-correlation in the frequency domain using Discrete Fourier Transform on Rotation Group on SO(3) (SOFT) is efficient and economical. Makadia et al. [10] illustrated the rotational alignment by EGI and suggested translational registration with cross-correlation of discrete occupancy grids. Rough alignment methods coupled with ICP can lead to a fully automatic registration of point clouds into a fixed reference frame.

Recently, scanners have been integrating the color information at the ranged point producing 3D color point clouds [11]. A color camera is combined with a 3D LIDAR ranging system can generate visually realistic and geometrically accurate representation of the scene. Several algorithms take advantage of the available color property to accelerate the map registration process and increase accuracy. Hue value from Hue-Saturation-Lightness (HSL) color model has been computed and utilized in all iterations during the ICP registration process [12]. Color data on depth image can be used to estimate initial alignment of a scans pair with the Scale Invariant Feature Transform (SIFT) has been proposed as a variant of the ICP fine registration [13]. The Depth-interpolated Image Feature (DIFT) algorithm associates the corresponding points between two images and registers the color point clouds based on the extracted correspondences [14]. Probabilistic scan registration methods trace laser beam to exploit maximum range readings to increase likelihood of alignment. Color attribute has been applied as kernel extension in Normal Distributions Transform (NDT) process so that robustness is increased [15].

This paper presents a variant on the EGI for automatic coarse alignment. The registration process is fully automatic because it requires no manual pre-alignment or user identification of corresponding points. As more and more scans are registered, the size of the model point cloud increase and down sampling of the point clouds becomes necessary. Geo-
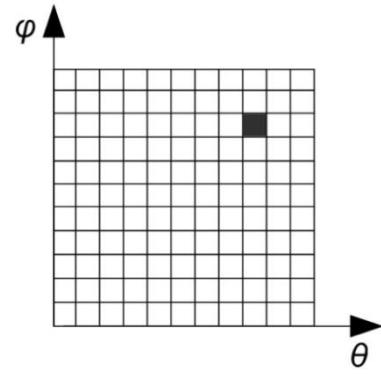
(a)
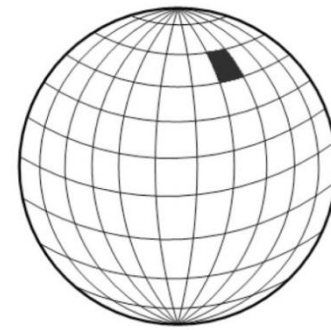
(b)

Figure 2. Surface point normal histogram representations: (a) surface normal histogram on the (θ, φ) plane, (b) surface normal histogram on EGI.

metry-based or sample density based down sampling techniques may indiscriminately cull points from overlapping areas. Since the hue information must match in the overlapping areas of the data (unregistered) and model (already registered) point clouds, hue filters designed with hue-distribution patterns of the data point cloud ensure that the points in the overlap areas in the model point clouds are preferentially retained. The traditional EGI algorithm for registration and hue filters used for selective clustering of points for EGI registration is described in the next section. A two scan matching scenario and an eight scan matching scenario are considered as illustrative examples. Performance measurements on the example scans are described in the third section. The paper concludes with remarks on the effectiveness of using hue filtering.

2. Hue assisted automatic registration algorithm

The automatic registration algorithm includes two parts: rotational alignment and translational alignment. Registration with the EGI follows the technique developed by Makadia et al. [10]. Rotational alignment is executed before translational alignment. A summary of rotational alignment based on EGI is presented for the sake of the completeness. The rotational alignment is solved by correlating point surface normal histograms from different point clouds in frequency domain.

Occupancy grids are built afterwards based on common bounding box and the 3D occupancy grids are expanded into 1D domain. Translation can then be computed based on the convolution results in frequency domain.
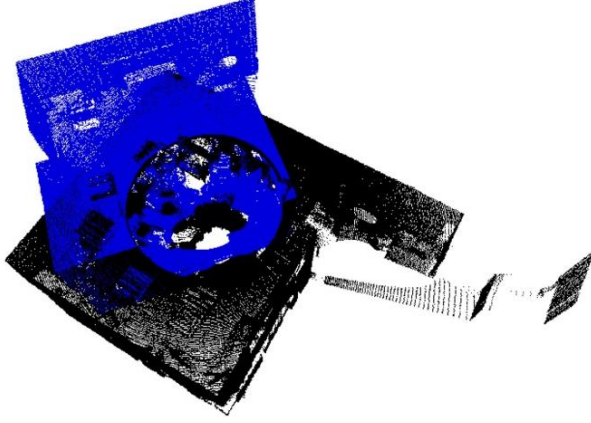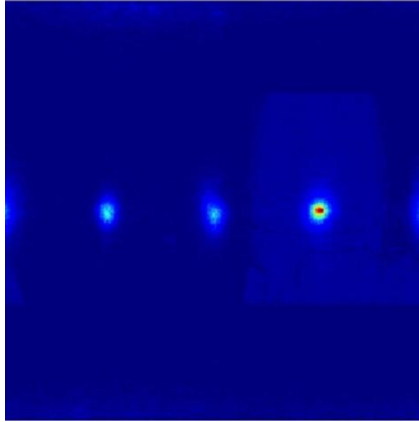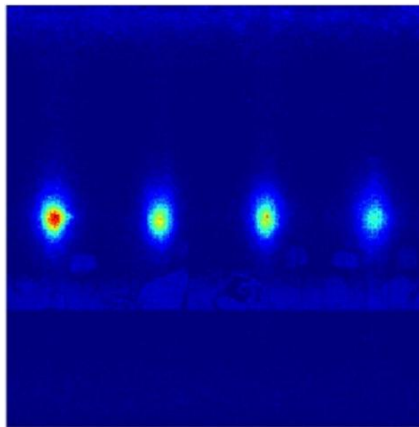

Figure 3. Model and data point clouds scanned from two separate vantage points of a conference room shown in their initial local coordinate systems.

(a)

(b)

Figure 4. Surface normal orientation histograms on the {θ, φ} plane: (a) data point cloud histogram, (b) model point cloud histogram.

2.1 Point cloud alignment with extended Gaussian images

2.1.1 Surface point normal histogram construction

Point cloud surface normal has been computed as the first step. There are several different algorithms such as Big Delaunay ball methods and Voronoi based methods [16] that can be applied to estimate the surface normal at each point in a point cloud. In this case point surface normal vector on single point has been computed by solving the nearest points fitted plane normal. Normal vector *n* can be represented by its orientation angle {θ, φ} in Figure 1 where are n_x, n_y and n_x, n_y and n_z are the directional cosines about the three orthogonal reference axes – X, Y and Z, respectively.

Surface normal orientation histogram can then be constructed after the normal computation at every point. A schematic representation of the orientation histogram $H(\omega)$ on (θ, φ) plane is shown in Figure 2(a), where $\omega \in SO(3)$. The Extended Gaussian Image (EGI) is formed as a unit sphere showing the surface normal vector orientation histogram projected on EGI as shown in Figure 2(b).

2.1.2 Rotational alignment with spherical Fourier transform

The rotation matrix *R* between data point cloud orientation histogram $H_d(\omega)$ and model point cloud orientation histogram $H_m(\omega)$ can be solved by computing the the rotation *R* required for maximum cross-correlation between $H_d(\omega)$ and $H_m(\omega)$. The correlation can be computed as shown in Eq. (1).

$$G(R) = \int_{\omega} H_m(\omega) H_d(R\omega) d\omega \tag{1}$$

The computational complexity of Eq. (1) scales with the square of number of samples in the orientation histogram and the size of the bins used for frequency counts. In order to improve the efficiency, a fast discrete Fourier Transform in SO(3) space was introduced [10] to solve the convolution of $H_d(\omega)$ and $H_m(\omega)$.

Following Ref. [10], using a set of spherical harmonic homogeneous polynomials, Y_n^l, of $2l + 1$ dimensions are used to generate an orthonormal basis for $H(\omega)$ with $\hat{h}_n^l$ as the coefficients of Spherical Fourier Transform (SFT). For a traditional ZYZ rotation sequence with Euler angles α, β and γ as the parameterization of the SO(3) rotation group, the coefficients of the SO(3) Fourier Transformation (SOFT) for a rotation, $R \in SO(3)$, can be determined as given by Eqs. (2)-(4). P_{mn}^l are the Associated Legendre Polynomials.

$$F(R) = \sum_{L \in N} \sum_{m=-l}^{l} \sum_{p=-l}^{l} \hat{f}_{mp}^l U_{mp}^l \tag{2}$$

$$\hat{f}_{mp}^l = \int_R f(R) \overline{U_{mp}^l(R)} dR \tag{3}$$

$$U_{mp}^l(R(\alpha, \beta, \gamma)) = e^{-im\gamma} P_{mn}^l(\cos(\beta)) e^{-in\alpha} \tag{4}$$
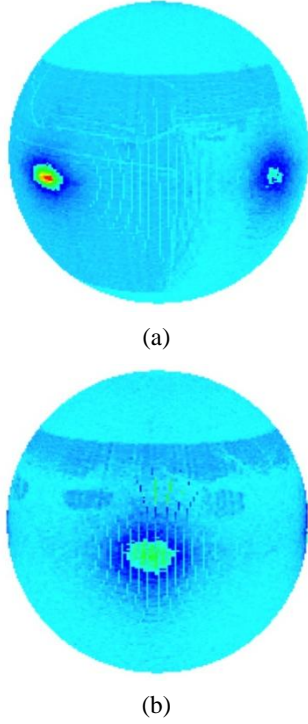
(a)

(b)

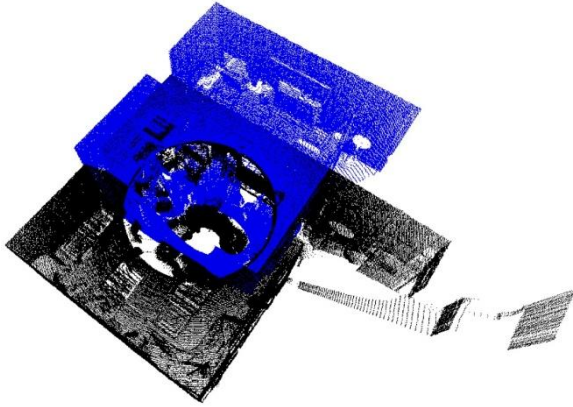Figure 5. Orientation histogram projected on EGI: (a) data cloud, (b) model cloud.

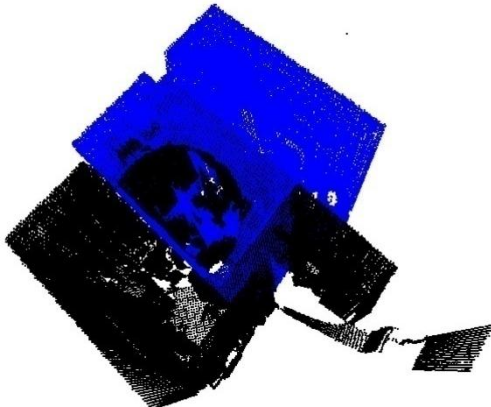Figure 6. Point clouds after rotational alignment with EGI.

Figure 7. Point clouds rendered on 3D occupancy grids.

Considering the SOFT coefficients of the model and data orientation histograms are defined as $\hat{h}_d^l$ and $\hat{h}_m^l$, respectively. The correlation of two spherical function can be obtained directly from the point-wise multiplication of the individual SOFT coefficients. The optimal rotational transformation (R) in Eq. (1) is determined by maximizing $\hat{G}_{dm}^l$.

$$\hat{G}_{dm}^l = \hat{h}_{dn}^l \hat{h}_{mn}^l \tag{5}$$

Inverse SOFT generates $G(R)$ with $2L + 1$ samples for each of the three Euler angles. The total complexity for computing $G(R)$ is of $O(L^3 \log^2 L)$.

2.1.3 Translational alignment with occupancy grid correlation

The translation matrix is computed by solving the correlation of occupancy grid between data and model point clouds after rotational alignment [17]. Bounding box of the occupancy grid used is the common bounding box encompassing both the model and data point clouds. The occupancy function is built by testing the existence of a scanned point in a uniformly sub-divided grid space.

$$Og(x, y, z) = \begin{cases} 1, & \text{if points exist} \\ 0, & \text{otherwise} \end{cases} \tag{6}$$

The 3D occupancy grid of data and model point clouds are shown as Figure 7. They can be stretched into 1D plane and shown as occupancy function $Og(\tau)$ in Figure 8. The correlation between data and model occupancy grids can be solved by

$$G(\mathbf{T}) = \int_{\tau \in R^3} Og_m(\tau) \, Og_d(\tau + \mathbf{T}) \tag{7}$$

The optimal transformation vector, $\mathbf{T}$, for correlation can be solved by maximizing the convolution of $Og_m(\tau)$ and $Og_d(\tau)$ as:

$$\mathbf{T} = \max\left[Real\left(\begin{matrix} InvFFT \\ \{FFT(Ogd(\tau)).FFT(Ogm(\tau))\} \end{matrix}\right)\right] \tag{8}$$

2.2 Illustration of EGI-based Registration

Two point clouds scanned from different vantage points in a conference room are shown, with coincident in their local coordinate system, in Figure 3. Data point cloud is shown in blue and model is shown in black. The point normal orientation histograms on (θ, φ) plane have been computed and shown in Figure 4. Orientation histograms projected on EGI are shown in Figure 5. After spherical correlation, data point cloud have been rotated and aligned with model point cloud, shown in Figure 6.

The correlation between $Og_m(\tau)$ and $Og_d(\tau)$ is shown as Figure 9. Data point cloud is then translated by T into model point cloud reference system. The result is shown in Figure 10.
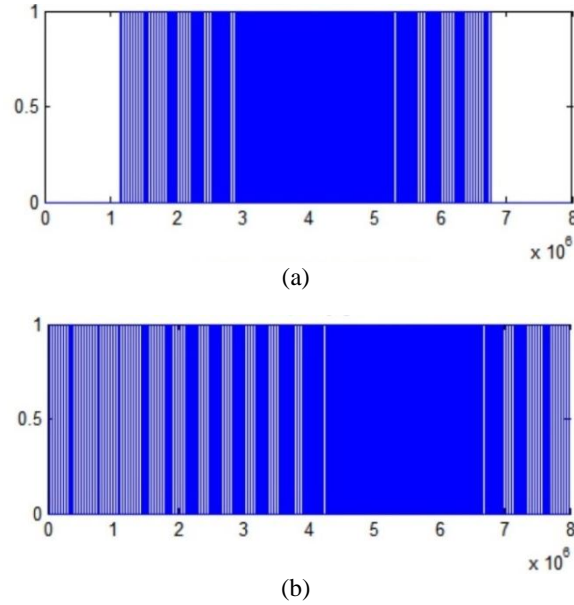
(a)

(b)

Figure 8. Binary 1-D representation of the occupancy grids: (a) data occupancy grid in 1D, (b) model occupancy grid in 1D.
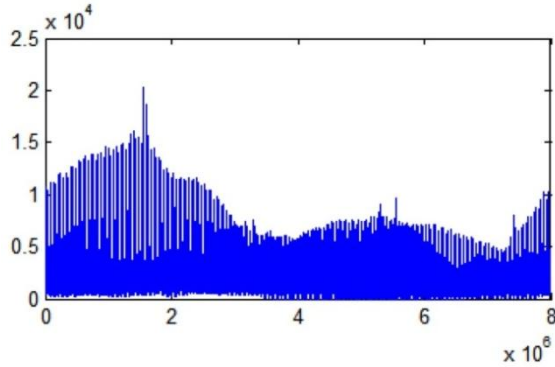

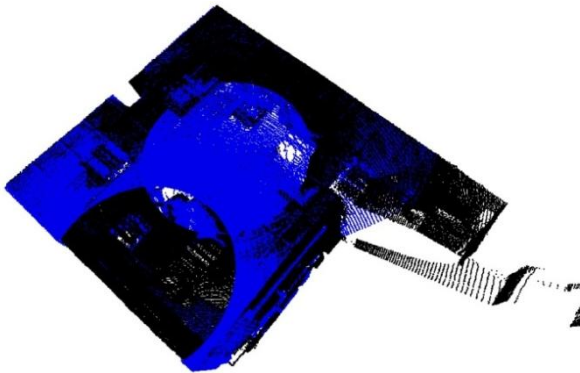Figure 9. Correlation after optimal translation of the occupancy grids.

Figure 10. Data point cloud registered into model reference system.

2.3 Hue-based point clustering

The registration speed and accuracy can be improved by taking advantage of the color attributes of the color point cloud. Color attributes on each point represent the visual characteristics of the scene. The color map of the scene is

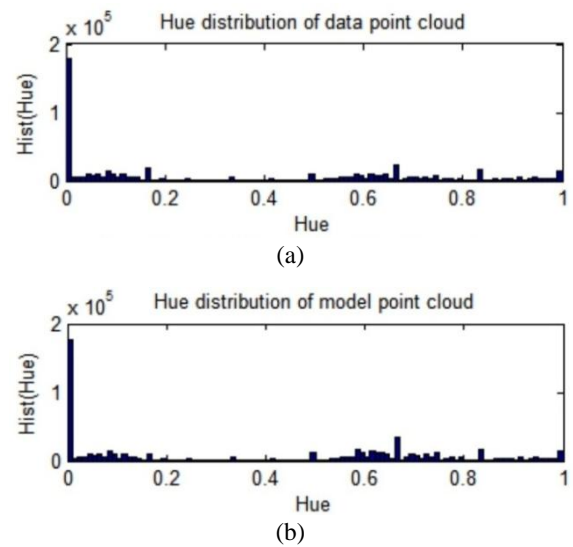Figure 11. Color point clouds scanned from two vantage positions.

(a)

(b)

Figure 12. Distribution of hue values for the model and data point clouds: (a) hue distribution of data point cloud, (b) hue distribution of model point cloud.
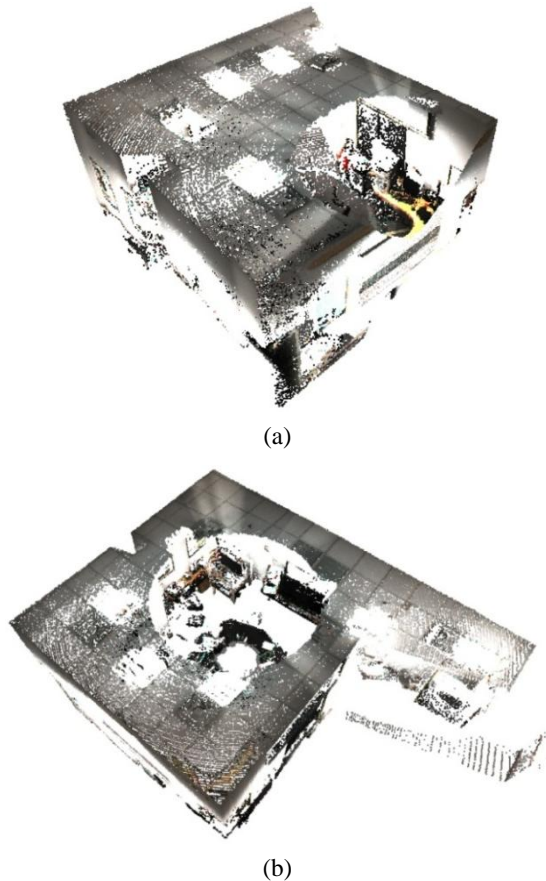
(a)

(b)

Figure 13. Hue-filtered color point clouds: (a) data color point cloud, (b) model color point cloud.
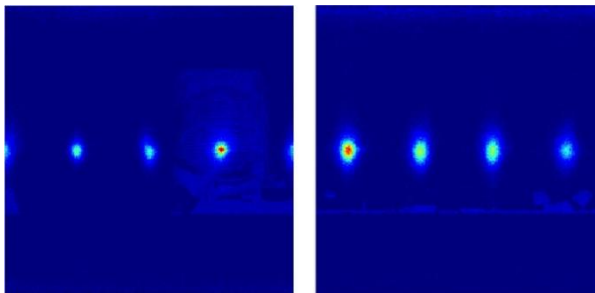

Figure 14. Orientation histogram of filtered point clouds.

typically independent of the underlying geometry, as an environment may be painted uncorrelated to the surface geometry. But for the exceptional cases in which the scene is entirely monochromatic, the sensed color information may provide additional cues during the association process. In most cases, lighting condition and camera orientation determines the {Red, Green, Blue} values in RGB color representation model. Hue value from Hue-Saturation-Lightness (HSL) is seen to be independent of the lighting and camera location [12]. Figure 11 shows the point clouds shown in Figure 3 with the additional color information. The hue distribution of data and model point clouds shown in Figure 11 are depicted in Figure 12. The hue distribution in HSL is generally computed from
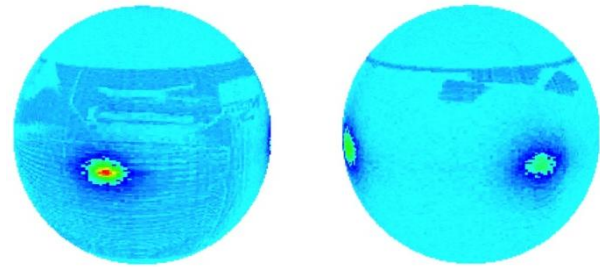

Figure 15. EGI of filtered point clouds.

Figure 16. Registration of the filtered point clouds.

$0°$ to $360°$. In this analysis the hue values are rescaled to a 0 to 1 scale by dividing the computed hue values by 360. However, the computed hue value will be zero ($H = 0$) when the color is red or when the red component (R) equals that of blue (B) and green components (G), i.e., $R = B = G$. Therefore, hue value is also zero for both black pixels and white pixels. Since a value of $H = 0$ is non-discriminating between reds, blacks and whites, further classification of this cluster of points may be necessary. For this illustration, we included the points with hue clustered around the zero value and the scene is known to have ceiling and wall areas that were painted white.

With the assumption that the hue values remain invariant with the scanner location and pose, the points scanned in overlapped areas must have the same hue distributions in the model and data point clouds.

An examination of the hue distributions provides insight into potential filter choices that will yield large number of filtered points in the overlap regions. One can consider a low pass filter with a hue value of less than 0.2 and another is a band pass filter with hue values between 0.5 and 0.85.

Other filters based on the inherent camera noise and sensitivity may also be used to select the hue filter. In Figure 12, most points hue value are between 0 to 0.5, filtering out high hue value point reduces the points for registration and consequently reduces the computational time. Both color property and 3D coordinates are kept after filtering for computation rigid rotation and translation. The hue values are used for registration accuracy computations. The filtered point clouds after applying a low pass hue filter ($h_f <= 0.5$) are shown in Figure 13. The number of points in the data point cloud was

Figure 17. Color point clouds generated at 8 different vantage positions in building hallway.

reduced from 597270 to 353386 and the number of points in the model point cloud was reduced from 631400 to 330832. The rendering of the model and data point clouds in Figure 13 shows that most of the scanned are was represented. The orientation histogram after hue filtering is shown in Figure 14 and after projection into an EGI is shown in Figure 15. Figure 16 shows the registered model and data point clouds.

2.4 Registration algorithm with hue-based filtering

The hue assisted automated color point cloud registration algorithm can be summarized as follows:

1. Load data point cloud P_d and model point cloud P_m;
2. Compute hue at every point in P_d and P_m;
3. Compute hue distributions for P_d and P_m; Design a hue filter that increases point sampling in the overlap areas of the point cloud.
4. Filter outlier and voxel de-sampling on both P_d and P_m;
5. Compute point surface normal $n_d\{1...N_d\}$ on data point cloud P_d and $n_m\{1...N_m\}$ on model point cloud P_m;
6. Construct orientation histogram H_d and H_m based on extracted point normal;
7. Solve rigid rotation matrix R by solving the correlation between H_d and H_m with SOFT(3);
8. Rotate P_d with R, get P_d';
9. Building occupancy grid with common bounding box in P_d' and P_m;
10. Solving rigid translation T by solving the convolution of P_d' and P_m,
11. Save transformed P_d' for fine registrations.

2.5 Error measurement

The registration error is measured by average distance between 2 nearest points from data to model point clouds, as defined in Eq. (9).

$$\in = \frac{1}{N} \sqrt{\begin{array}{l}(x_{id} - x_{im})^2 + (y_{id} - y_{im})^2 \\ + (z_{id} - z_{im})^2 + (H_{id} - H_{im})^2\end{array}} \tag{9}$$
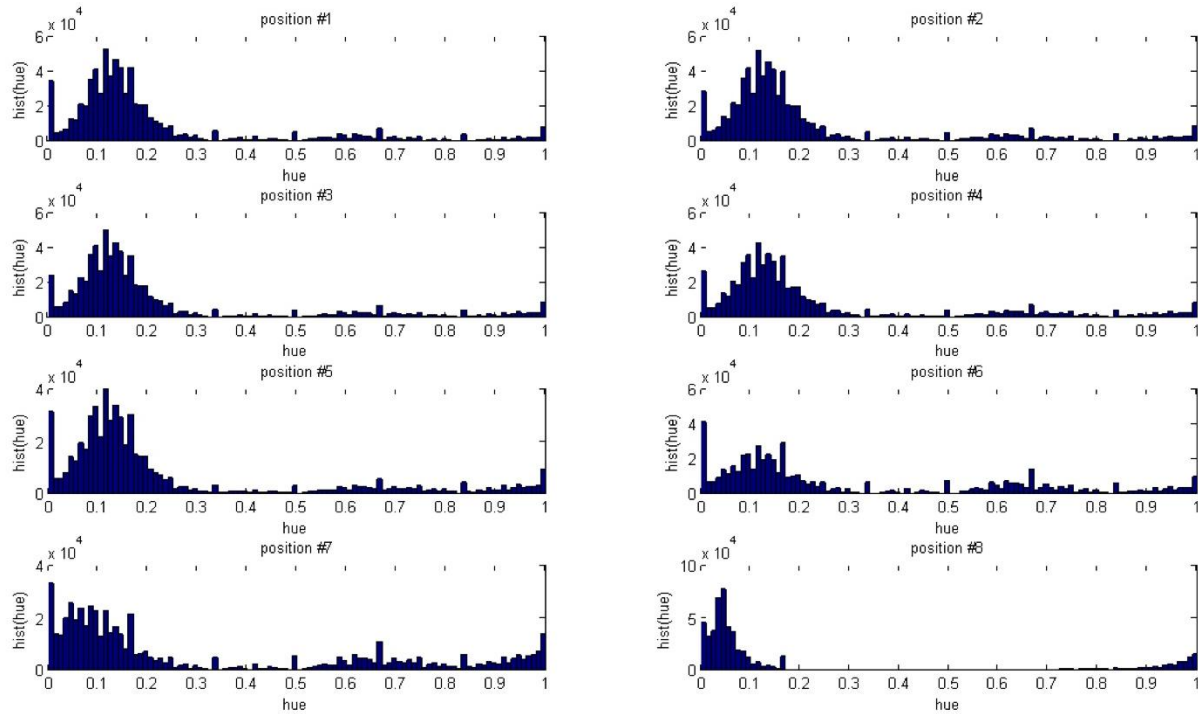
Figure 18. Hue distribution histogram for 8 color point clouds.

Figure 19. Eight scans aligned to form a complete map a building hallway with approximately five million points.

Figure 20. Color point clouds after registration.

The error is computed between point $p_{id}\{x_{id}, y_{id}, z_{id}\}$ in the data point cloud and its nearest neighbor point $p_{im}\{x_{im}, y_{im}, z_{im}\}$ in the model point cloud. Two points are paired when distance between p_{id} and p_{im} $\text{dist}(p_{id}p_{im}) < r_l$. r_l is a small constant value to chosen to ensure two nearest points are matched only within certain distance. N is the total number of paired points.

The computational time required for the registration of the two example color point clouds with hue-based filtering was 22.599 seconds and error is 0.001482. Using the same computational hardware, the registration with EGI based rotational and occupancy grid based translational registration but without the hue filtering took 31.572 seconds and produced an error of 0.001501. The Hue filtered EGI method was faster and produced more precise alignment.

3. Results for multi-scan registration

The second example considered for performance measurement was the registration of eight color point clouds generated at different vantage positions. Both EGI based and EGI with hue-filtering methods were considered. The eight sepa-
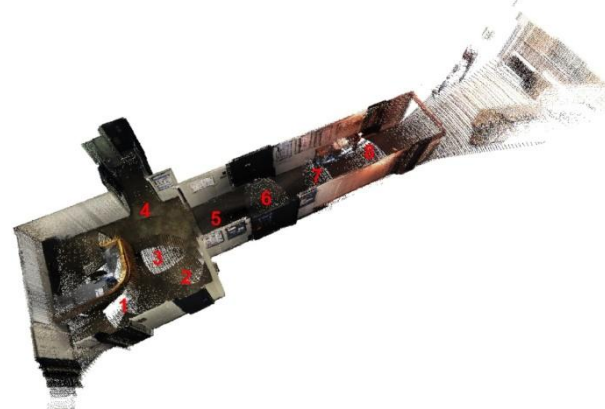
rate color point clouds are shown in Figure 17. They each have a partial coverage of the whole area and considerable overlap between consecutively numbered point clouds. Hue distributions for the point clouds are calculated and shown in Figure 18. Based on the hue-distributions seen in Figure 18, a hue constraint placed with a low pass filter ($h_f <= 0.5$).

The vantage positions are numbered as shown in Figure 19. The reference coordinate system of position-3 was arbitrarily selected as the global reference coordinate system. The other point clouds were registered into reference coordinate system established at position-3. The computation time and registration error for registering each of the other point clouds in sequence to point cloud at position-3 are tabulated in Table 1. Experimental results show that the hue assisted registration algorithm provides a reliable improvement in both computation time and registration accuracy.

Table 1. Registration results comparison.

Position	Traditional EGI		Hue assisted EGI	
	Time (sec)	Error	Time (sec)	Error
1	35.270	0.003326	32.742	0.003098
2	35.445	0.002398	32.251	0.002326
4	35.464	0.001586	30.845	0.001581
5	36.982	0.002108	29.838	0.002089
6	34.743	0.003378	28.353	0.001943
7	32.798	0.003087	27.971	0.003016
8	33.440	0.008274	29.822	0.008274
Average	34.877	0.00363	30.260	0.00319

A global color point clouds map is constructed after registering the seven color point clouds into the reference coordinate system set up by position-3. A 3D view of the complete space after registration into a single coordinate system is shown in Figure 20. This coarse registration results can then be supplied for fine registration such as ICP to produce higher quality registration. Both computational time and error are reduced and the filtering helps to decrease the number of points into rigid transformation computation, which is a great advantage in registration process. Hue filtering also helps to increase registration accuracy because clustering similar point together is essentially keeping common points and filtering out uncommon points between color point clouds.

4. Conclusions

A hue assisted automatic coarse registration algorithm that solves correlation for spherical rotation and 3D translation is described in this paper. The hue distributions in the color point clouds have been analyzed and hue filters were used to down sample the number of points used for registration. A set of color point clouds of a long hallway in a building and a conference room were registered with traditional EGI and after applying hue-based filters. The use of the hue filters is shown to accelerate the registration speed and reduce registration error. Although the improvements in the registration speed for the example data sets is seen to be about 20%, better hue filter designs can potentially lead to further down sampling of points and acceleration of various steps in the registration. Since no manual intervention or pre-alignment is necessary, this methodology can used as a coarse alignment step before using ICP methods for fine registration.

References

[1] Thrun S. Robotic mapping: a survey. Exploring artificial intelligence in the new millennium. Morgan Kaufmann Publishers Inc.; 2003. p. 1-35.

[2] Bsel PJ. A method for registration of 3-D shapes. IEEE Trans on Pattern Analysis and Machine Intelligence; 1992; 14(2): 239-256.

[3] Rusinkiewucz S, Levoy M. Efficient variants of the ICP algorithm. In: Proceedings of the 3rd International Conference on 3-D Digital Imaging and Modeling; 2001 May 28-Jun 1; Quebec City, Canada; pp. 145-152.

[4] Jost T, Hügli H. Fast ICP algorithms for shape registration. Lecture Notes in Computer Science. 2002; 2449: 91-99.

[5] Low K. Linear least-squares optimization for point-to-plane ICP surface registration. Technical Report of University of North Carolina. 2004 Feb; 3 p. Report No. TR04-004.

[6] Lorusso A, Eggert DW, Fisher RB. A comparison of four algorithms for estimating 3D rigid transformations. In: Proceedings of the British Machine Vision Conference, 1995 Sep 11-14; Birmingham, UK; p. 237-246.

[7] Johnson A. Spin-images: a representation for 3D surface matching. Ph.D. Thesis. 1997; Carnegie Mellon University, USA.

[8] Chung D, Lee YDS. Registration of multiple range views using the reverse calibration technique. Pattern Recognition. 1998; 31(4); 457-464.

[9] Brunnstrom K, Stoddart A. Genetic algorithms for free-form surface matching. In: Proceedings of the International Conference of Pattern Recognition, 1996 Aug 25-29; Vienna, Austria; p. 689-693.

[10] Makadia A, Patterson A IV, Daniilidis K. Fully automatic registration of 3D point clouds. In: Proceedings of the 2006 Computer Society Conference own Computer Vision and Pattern Recognition; 2006 Jun 17-22; New York, NY; p. 1297-1304.

[11] Gebre B, Men H, Pochiraju K. Remotely operated and autonomous mapping system (ROAMS). In: Proceedings of the 2nd Annual IEEE International Conference on Technologies for Practical Robot Applications; 2009 Nov 9-10; Woburn, MA; p. 173-178.

[12] Men H, Gebre B, Pochiraju K. Color point cloud registration with 4D ICP algorithm. In: Proceedings of the IEEE International Conference on Robotics and Automation; 2011 May 9-13; Shanghai, China; p. 1511-1516.

[13] Andersson H. Vision aided 3D laser scanner based registration. In: Proceedings of the European Conference on Mobile Robots (ECMR); 2007 Sep 19-21; Freiburg, Germany; p. 192-197.

[14] Nuchter A. 6D SLAM with approximate data association. In: Proceedings of the IEEE International Conference on Robotics and Automation; 2005 Apr 18-22; Barcelona, Spain; p. 242-249.

[15] Salvi J, Matabosch C, Fofi D, Forest J. A review of recent range image registration methods with accuracy evaluation. Image and Vision Computing. 2007; 25(5): 578-596.

[16] Chua CJR. Point signatures: a new representation for 3D object recognition. International Journal on Computer Vision. 1997; 25(1): 63-85.

[17] Kostelec PJ, Rockmore DN. FFT on the rotation group. Journal of Fourier Analysis and Application. 2008; 14(2): 145-179.